

## Supplementary Information

### Self-supported Ni/Ni<sub>3</sub>N<sub>1-x</sub> Heterostructures with Abundant Nitrogen Vacancies as Efficient Electrocatalysts for Ethylene Glycol Oxidation

Chenyu Zhou <sup>a,1</sup>, Chenghao Jia <sup>a,1</sup>, Xuepeng Xiang <sup>a,b</sup>, Luolan Wang <sup>a</sup>, Shiyong Wu <sup>a</sup>, Nian Zhang <sup>c</sup>, Shijun Zhao <sup>b</sup>, Gaixiu Yang <sup>d</sup>, Yan Chen <sup>a,\*</sup>

<sup>a</sup> State Key Laboratory of Pulp and Paper Engineering, School of Environment and Energy, South China University of Technology Guangzhou, Guangdong 510006, P. R. China

<sup>b</sup> Department of Mechanical Engineering, City University of Hong Kong, Hong Kong, China.

<sup>c</sup> State Key Laboratory of Functional Materials for Informatics, Shanghai Institute of Microsystem and Information Technology, Chinese Academy of Sciences, Shanghai, 200050, P. R. China

<sup>d</sup> Guangzhou Institute of Energy Conversion, Chinese Academy of Sciences, Guangzhou, 510640, PR China

<sup>1</sup> These authors contribute equally to this work

\* Corresponding author

\* E-mail addresses:

[escheny@scut.edu.cn](mailto:escheny@scut.edu.cn) (Prof. Y. Chen.)

## 1. Supplementary Notes

### Text S1: Chemicals

Hydrochloric acid (HCl, 37 wt.%) was obtained from Guangzhou Chemical Reagent Factory (China). Potassium hydroxide (KOH, 85%) was obtained from Tianjin Damao Chemical Reagent Factory (China). Anhydrous ethylene glycol (CH<sub>2</sub>OH-CH<sub>2</sub>OH, 99%) and formic acid (HCOOH, 99%) were obtained from Shanghai

Macklin Biochemical Co., Ltd. Q. Macroporous nickel foam (110 ppi with the mass density of 320 g·m<sup>-2</sup>) supplied by Suzhou Suneruo Technology Co., Ltd. All aqueous solutions were prepared with deionized water with a resistivity of 18.25 MΩ cm<sup>-1</sup>.

### **Text S2: In-situ Fourier Transform Infrared (in-situ FT-IR) Measurement**

In-situ FT-IR measurements were performed on a Nicolet-6700 spectrometer (Thermo Fisher Scientific, America) with a scanning number of 32 at a resolution of 4 cm<sup>-1</sup> (0.2 min per spectrum), and the HgCdTe (MCT/A) detector which needed to be cooled by liquid nitrogen. Chronoamperometry testing under 0.5 V (vs. Ag/AgCl) during FT-IR testing was based on external electrochemical components. The electrochemical test was performed by using a CHI-660E electrochemical station in a custom-made three-electrode electrochemical single cell.

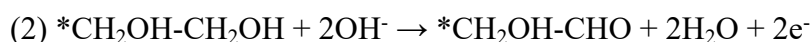
### **Text S3: Products analysis**

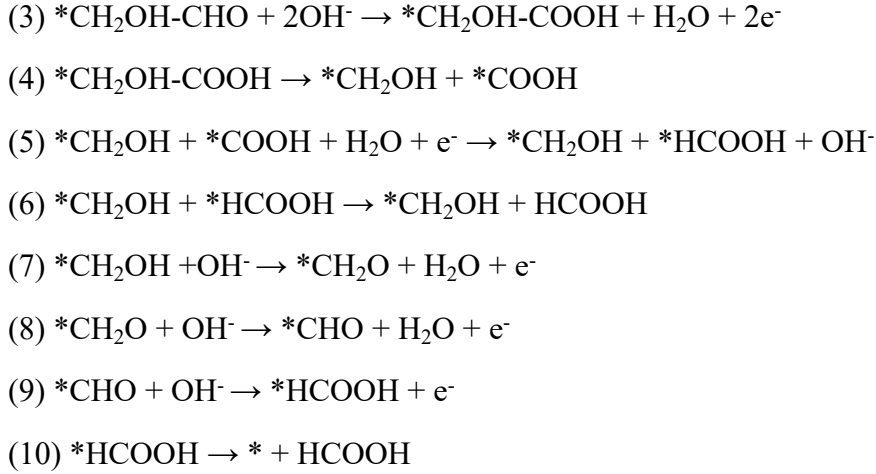
The concentrations of EG were determined by HPLC equipping with Sugar-H column, and the mobile phase was H<sub>2</sub>SO<sub>4</sub> (pH=2.5±0.1) with the flow rate of 0.5 ml/min at 45 °C. The concentration of formate was tested by HPLC equipping with the ultraviolet-visible detector. Chronoamperometry test were carried out at a constant potential of 0.5 V (vs. Ag/AgCl) in 15 mL 1 M KOH with 0.3 M EG. 2 μL electrolyte was extracted and then diluted to 2 mL for measurement. Corresponding calibration curves of EG and formate as shown in Figure S18. The Faradaic efficiency (FE) and formate selectivity were calculated with the following equations:

$$FE(\%) = \frac{\text{mole of produced formate}}{\text{total charge passed}/(n \times 96485 \text{ C mol}^{-1})} \times 100\%$$

$$\text{Selectivity} = \frac{\text{mole of produced formate}/2}{\text{mole of converted EG}} \times 100\%$$

### **Text S4: The reaction steps of EGOR calculation in alkaline solution**





where “\*” donates as the adsorption sites, which are generally the exposed metal sites.

The configurations of EGOR pathway are shown in Fig. 4d. The Gibbs free energy changes of each step are calculated by:

$$\Delta G_1 = G(\text{*CH}_2\text{OH-CH}_2\text{OH}) - G(\text{*}) - G(\text{CH}_2\text{OH-CH}_2\text{OH})$$

$$\Delta G_2 = G(\text{*CH}_2\text{OH-CHO}) + G(\text{H}_2) - G(\text{CH}_2\text{OH-CH}_2\text{OH})$$

$$\Delta G_3 = G(\text{*CH}_2\text{OH-COOH}) + G(\text{H}_2) - G(\text{CH}_2\text{OH-CHO}) - G(\text{H}_2\text{O})$$

$$\Delta G_4 = G(\text{*CH}_2\text{OH}, \text{*COOH}) - G(\text{*CH}_2\text{OH-COOH})$$

$$\Delta G_5 = G(\text{*CH}_2\text{OH}, \text{*HCOOH}) - G(\text{*CH}_2\text{OH}, \text{*COOH}) - 0.5 G(\text{H}_2)$$

$$\Delta G_6 = G(\text{*CH}_2\text{OH}) + G(\text{HCOOH}) - G(\text{*CH}_2\text{OH}, \text{*HCOOH})$$

$$\Delta G_7 = G(\text{*CH}_2\text{O}) + 0.5 G(\text{H}_2) - G(\text{*CH}_2\text{OH})$$

$$\Delta G_8 = G(\text{*CHO}) + 0.5 G(\text{H}_2) - G(\text{*CH}_2\text{O})$$

$$\Delta G_9 = G(\text{*HCOOH}) + 0.5 G(\text{H}_2) - G(\text{*CHO}) - G(\text{H}_2\text{O})$$

$$\Delta G_{10} = G(\text{*}) + G(\text{HCOOH}) - G(\text{*HCOOH})$$

The energy of rate-determining step ( $G_{max}$ ) marked in Fig. 4d was calculated by the following formula:

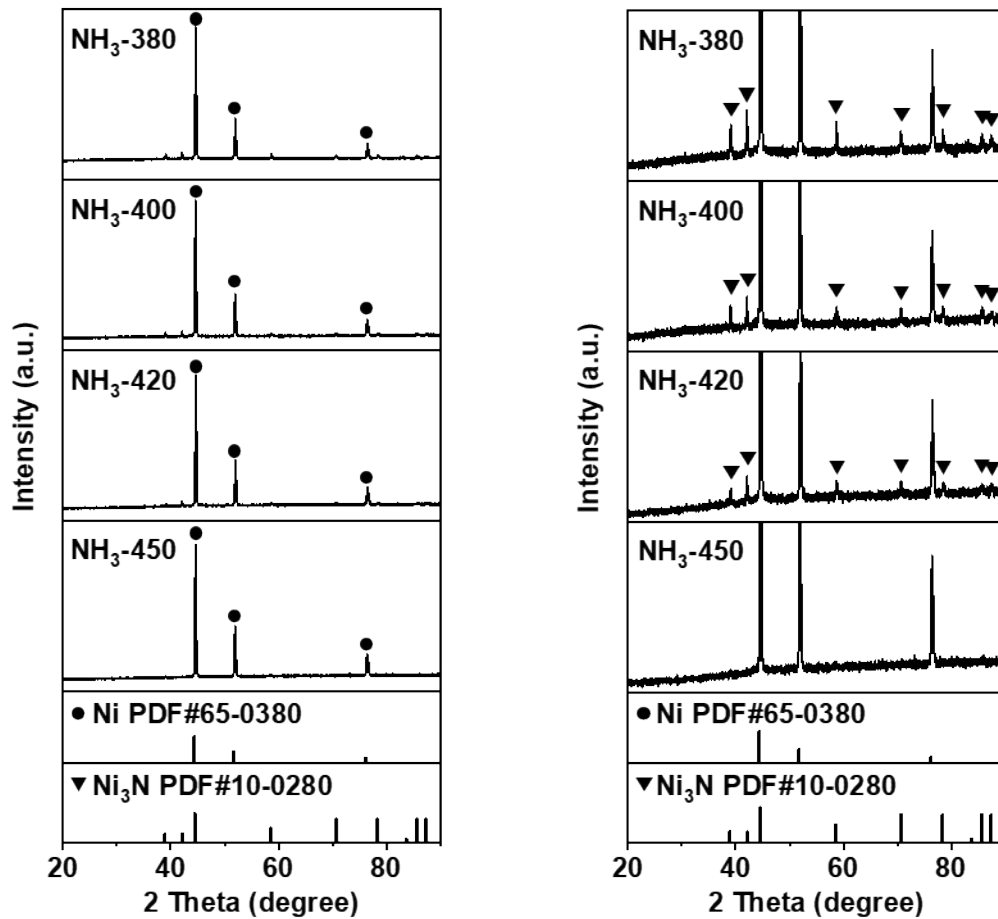
$$G_{max} = \text{Max} [\Delta G_1, \Delta G_2, \Delta G_3, \Delta G_4, \Delta G_5, \Delta G_6, \Delta G_7, \Delta G_8, \Delta G_9, \Delta G_{10}].$$

### **Text S5: Construction of structural model**

It is well known that the (111) plane is most stable surface of Ni, and there are two common exposed planes, (111) plane and (001) plane, for Ni<sub>3</sub>N. Through calculation,

Ni<sub>3</sub>N (111) plane had the lower energy (-497.30 eV) than (001) plane (-495.62 eV) which proved the better stability of the Ni<sub>3</sub>N (111) plane. Therefore, the Ni<sub>3</sub>N (111) slab was selected to form the Ni/Ni<sub>3</sub>N structure with the Ni (111) slab. In addition, the Ni<sub>3</sub>N slab was moved in the x, y, and z directions relative to the Ni slab to find the global energy minimum (Figure S11). There were two kinds of nitrogen sites on Ni/Ni<sub>3</sub>N. The energy of models with different nitrogen vacancies was calculated in order to determine the most stable configuration as the Ni/Ni<sub>3</sub>N<sub>1-x</sub> (Figure S12).

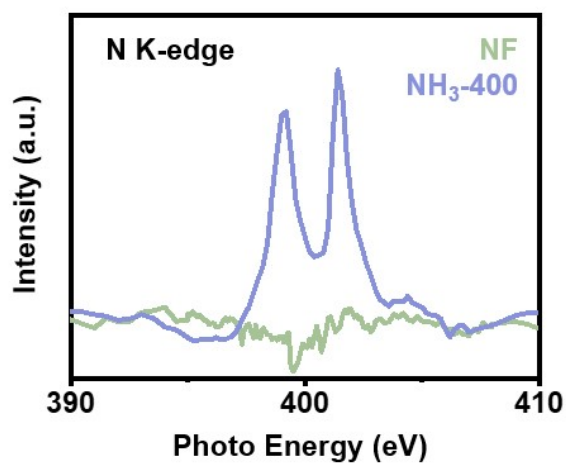
## 2. Supplementary Figures



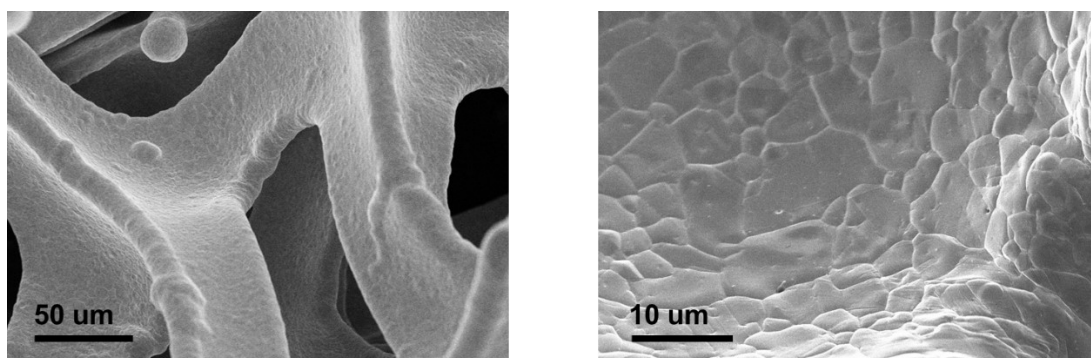
**Figure S1.** XRD patterns of the Ni/Ni<sub>3</sub>N<sub>1-x</sub> samples at different nitridation temperature.



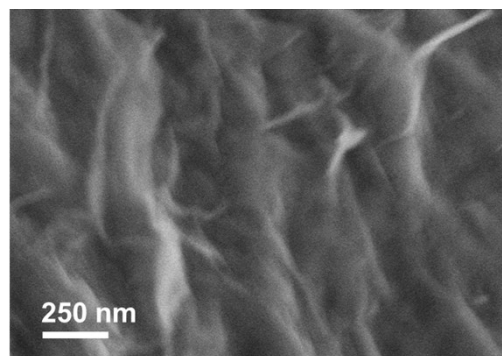
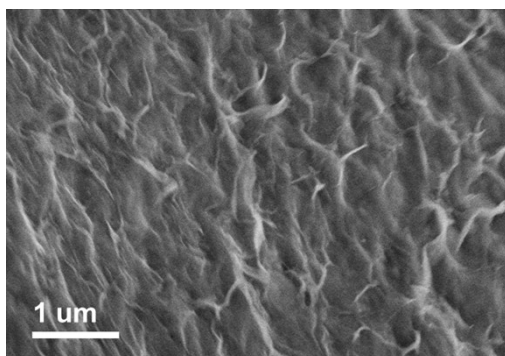
**Figure S2.** Representative photo of the samples subjected to nitridation temperature of 420 °C.



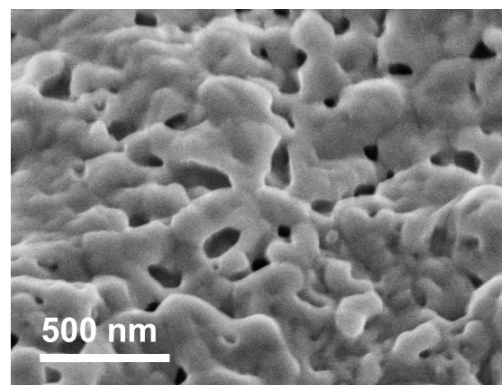
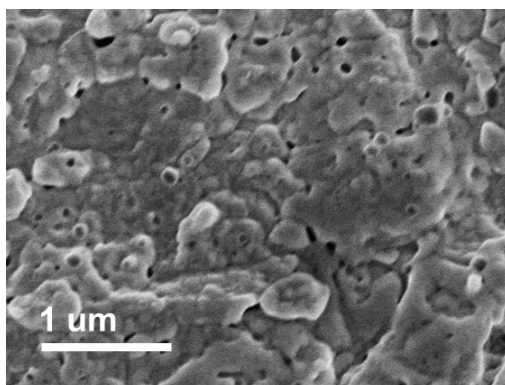
**Figure S3.** N K-Edge sXAS spectra of NF and NH<sub>3</sub>-400 sample



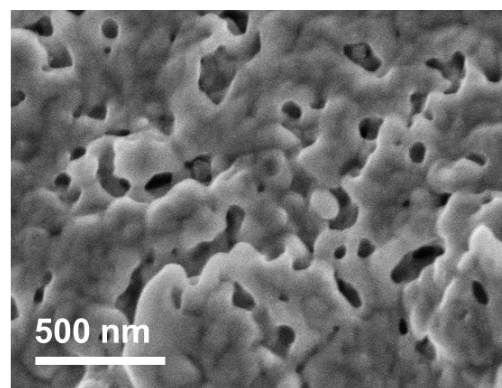
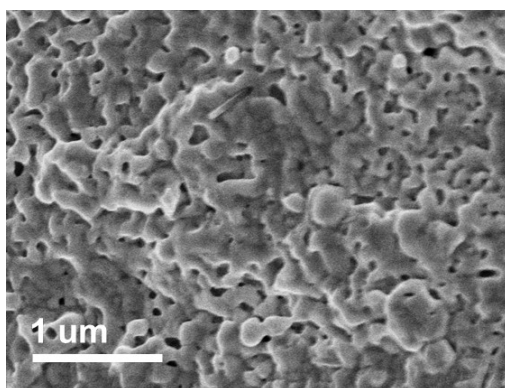
**Figure S4.** SEM images of Ni



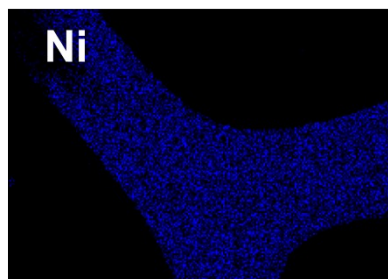
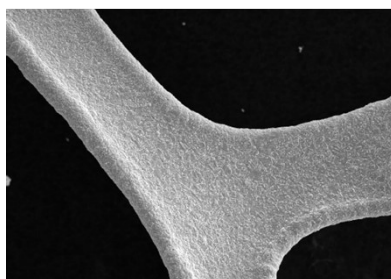
**Figure S5.** SEM images of Ni(OH)<sub>2</sub>/Ni



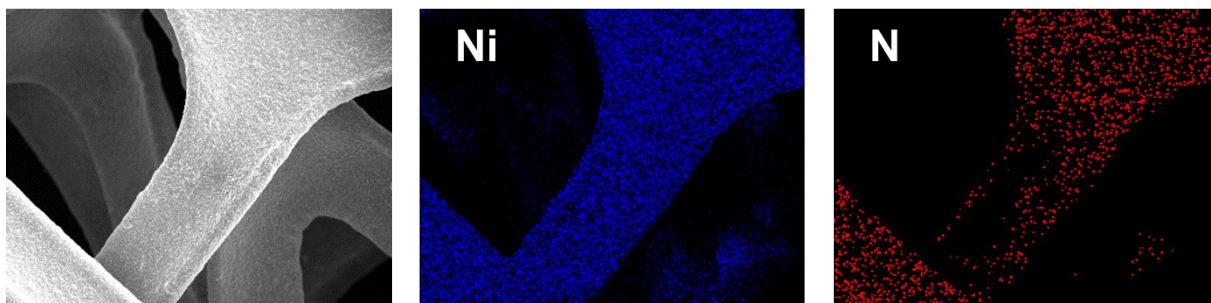
**Figure S6.** SEM images of NH<sub>3</sub>-380



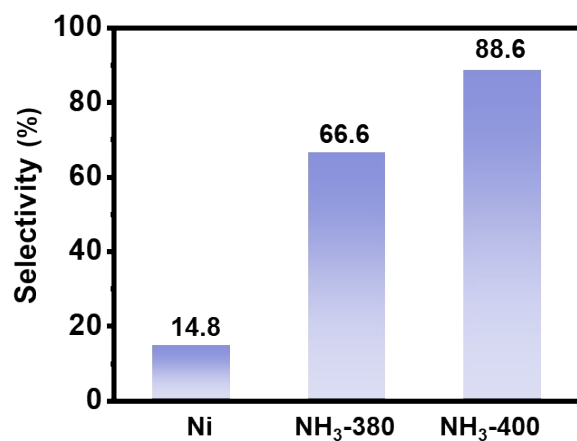
**Figure S7.** SEM images of NH<sub>3</sub>-400



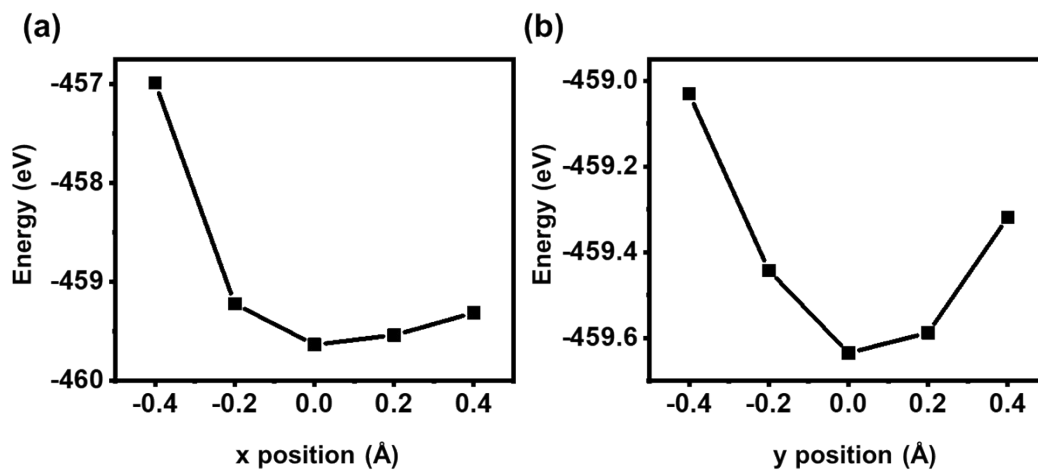
**Figure S8.** EDS mapping of NH<sub>3</sub>-380 sample



**Figure S9.** EDS mapping of NH<sub>3</sub>-400 sample



**Figure S10.** The formate selectivity of the NH<sub>3</sub>-k samples electrolyzed for 60 min and the Ni sample electrolyzed for 6 h at a voltage of 0.5V (vs. Ag/AgCl)



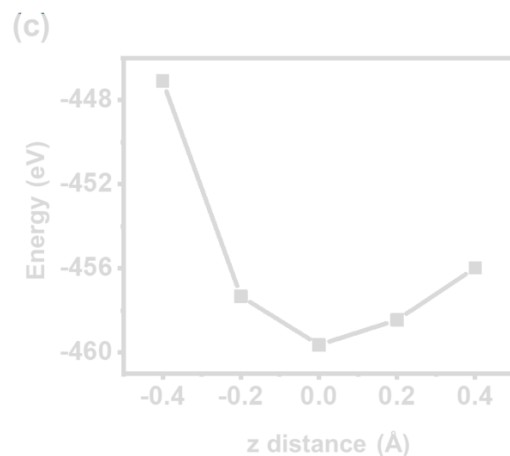


**Figure S11.** The movement test of Ni/Ni<sub>3</sub>N interface model in (a) x, (b) y and (c) z direction

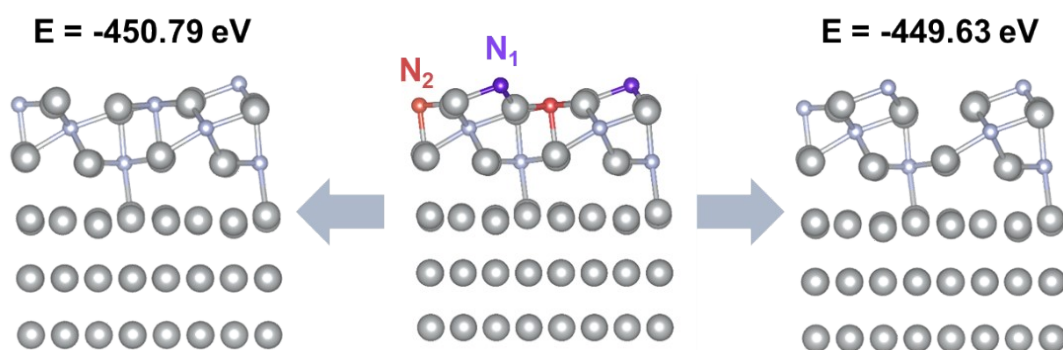


**Figure S12.** The structures and energy of Ni/Ni<sub>3</sub>N<sub>1-x</sub>

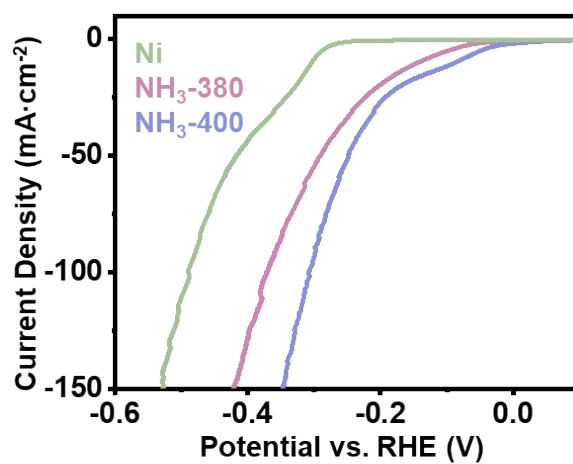


**Figure S13.** LSV curves of pristine Ni, NH<sub>3</sub>-380 and NH<sub>3</sub>-400 samples

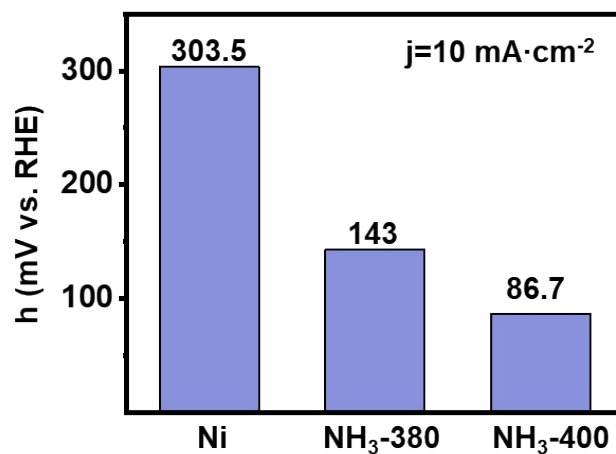


**Figure S14.** Overpotentials at the current density of  $10 \text{ mA cm}^{-2}$  of pristine Ni, NH<sub>3</sub>-380 and NH<sub>3</sub>-400 samples

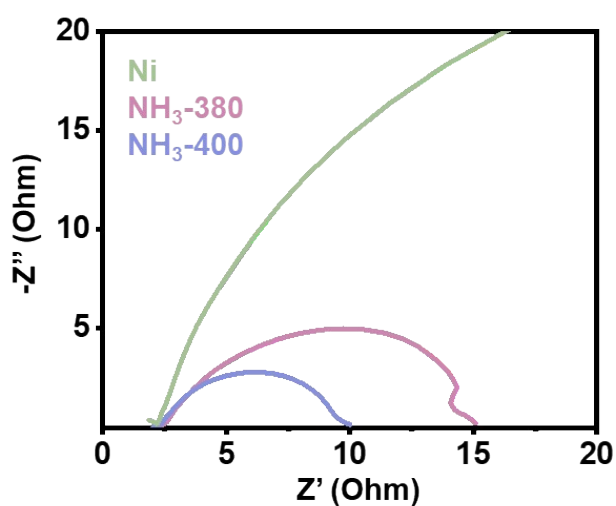


**Figure S15.** EIS spectra of pristine Ni, NH<sub>3</sub>-380 and NH<sub>3</sub>-400 samples

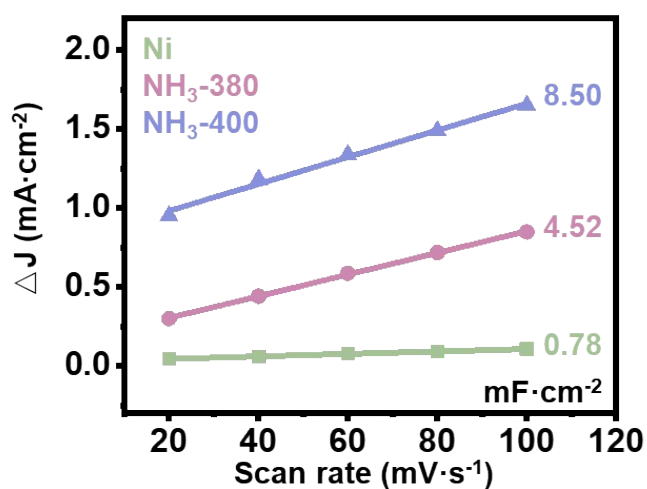


**Figure S16.**  $C_{dl}$  values pristine Ni, NH<sub>3</sub>-380 and NH<sub>3</sub>-400 samples

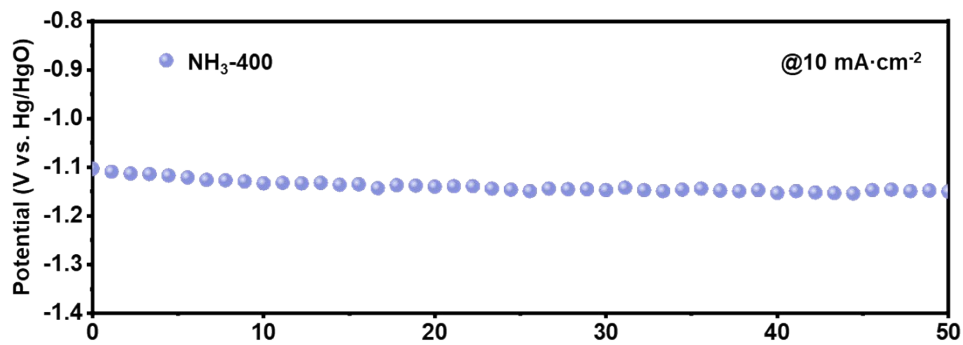


**Figure S17.** Chronopotentiometry curves for NH<sub>3</sub>-400 acquired in 1 M KOH electrolyte at the current density of 10 mA cm<sup>-2</sup>.

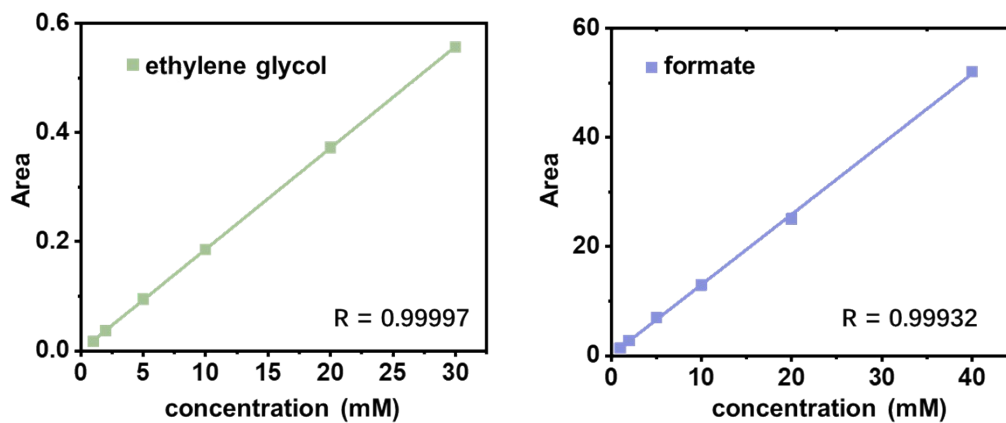


**Figure S18.** The corresponding calibration curves of EG and formate

### 3. Supplementary Tables

**Table S1.** The peak-splitting information about Ni 2p XPS spectra

| species              | Ni <sup>0</sup> | Ni <sup>1</sup> | Ni <sup>2</sup> | Ni <sup>3</sup> | Sta.     |
|----------------------|-----------------|-----------------|-----------------|-----------------|----------|
| Ni                   | 852.2 eV        | 853.5 eV        | 855.2 eV        | /               | 860.1 eV |
|                      | 869.7 eV        | 871.0 eV        | 872.4 eV        |                 | 878.2 eV |
| NH <sub>3</sub> -380 | 852.6 eV        | 853.6 eV        | 855.7 eV        | 857.4 eV        | 867.1 eV |
|                      | 869.9 eV        | 872.1 eV        | 873.7 eV        | 875.9 eV        | 879.7 eV |
| NH <sub>3</sub> -400 | 852.0 eV        | 852.9 eV        | 855.1 eV        | 856.9 eV        | 860.5 eV |
|                      | 869.3 eV        | 871.3 eV        | 873.0 eV        | 875.2 eV        | 878.9 eV |

**Table S2.** The proportion of N 1s XPS spectra for NF, NH<sub>3</sub>-380 and NH<sub>3</sub>-400 samples

| species              | Ni-N bond | N-vacancy | N-O bond |
|----------------------|-----------|-----------|----------|
| NH <sub>3</sub> -380 | 59.5%     | 26.9%     | 13.6%    |
| NH <sub>3</sub> -400 | 47.0%     | 42.3%     | 10.7%    |